Turkish Journal of Electrical Engineering & Computer Sciences

http://journals.tubitak.gov.tr/elektrik/

Research Article

Turk J Elec Eng & Comp Sci
(2018) 26: 2260 – 2274

doi:10.3906/elk-1712-215

A noninvasive time-frequency-based approach to estimate cuffless arterial blood pressure

Ömer Faruk ERTUĞRUL, Necmettin SEZGİN*
Department of Electrical and Electronics Engineering, Faculty of Engineering and Architecture,
Batman University, Batman, Turkey

Received: 16.12.2017 • **Accepted/Published Online:** 06.07.2018 • **Final Version:** 28.09.2018

Abstract: Arterial blood pressure (ABP) is one of the most vital signs in the prophylaxis and treatment of blood pressure-related diseases because raised blood pressure is the most significant cause of death and the second major cause of disability in the world. Higher ABP yields greater strain on arteries and these extra strains turn arteries into thicker, less flexible, and more narrow structures. This increases the possibility of having an artery busting or artery occlusion, which are the primary reasons for heart attacks, kidney disease, or strokes. In addition to its importance in monitoring cardiovascular homeostasis, measurement of ABP is imperative in surgical operations. In this study, a simple and effective approach was proposed to estimate ABP from electrocardiogram (ECG) and photoplethysmograph (PPG) signals by an extreme learning machine (ELM) and statistical properties of the ECG and/or PPG signals in the time-frequency domain. To evaluate and apply the proposed approach, the Cuffless Blood Pressure Estimation Dataset, which was published and shared by UCI, was employed. First, the statistical properties were extracted from ECG and PPG signals that were in the time-frequency domain. Later, extracted features were employed to estimate cuffless ABP for each subject by the ELM and some popular machine learning methods. Achieved results and reported results in the literature showed that the proposed approach can be successfully employed for estimating cuffless blood pressure (BP) from ECGs and/or PPGs. Additionally, with the proposed approach, the systolic BP, mean BP, and diastolic BP can be calculated simultaneously.

Key words: Cuffless artificial blood pressure, extreme learning machine, time-frequency analysis, statistical variables, electrocardiogram, photoplethysmograph

1. Introduction

Blood pressure (BP) shows the pressure of blood in the arteries. High BP (generally higher than 140/90 mmHg), which is also called hypertension, greatly increases the risk of heart problems and some other illness [1]. It was reported that it is not only the largest cause of mortality but also the biggest risk factor for coronary heart disease and disabilities [2]. This risk can be reduced by simply changing lifestyle, going on a diet, or being the right weight for height. Although it is an essential parameter in human health, for more than a century, it has been generally measured by mercury sphygmomanometer around the arm or leg based on auscultation and a manometer. Some indirect BP measurement methods have been proposed and employed successfully, but it was reported that utilizing the mercury sphygmomanometer still showed higher accuracy than these indirect measurement methods [2].

*Correspondence: necmettin.sezgin@batman.edu.tr

Although measuring BP by mercury sphygmomanometer is more accurate, it is time-consuming and also hard or impossible to measure continuously [3]. For some cases, for example, in surgical operations or during exercises, measuring BP continuously by a mercury sphygmomanometer is impractical or impossible [4]. Therefore, some methods have been proposed to estimate BP by electrocardiogram (ECG) and/or photoplethysmograph (PPG) [4–7]. Pulse transit time (PTT), pulse arrival time (PAT), and heart rate (HR) are generally employed methods in the estimation of BP [4,5,8].

Although PTT was successfully employed in the literature [9–12], it has many drawbacks. Since PTT shows the time interval between the peak of the R-wave of an ECG and a characteristic point of a PPG, to obtain a PTT signal both ECG and PPG signals are required [6,13,14]. Additionally, it is not a subject-free method and it is based on individual physiological properties of the subject. Therefore, it requires calibration for each subject [15,16]. Furthermore, it was reported that PTT can successfully track the variations of high-frequency components of BP that are caused by activities [13], but it does not show the same ability in tracking low-frequency variations.

To overcome these drawbacks, in this study a novel and a simple approach is proposed. Although PTT shows the time interval between specific peaks, it can be said that it has a link with the time-frequency representation of the signal [17–19], because the peaks cause a specific component in the frequency domain and both the times at which the peaks occurred can be observed in the time-frequency domain. Although the extreme learning machine (ELM) is a training method in single hidden layer artificial neural networks, it has an extremely fast training stage with a high generalization capacity [20–24]. Therefore, the statistical properties of ECG and PPG signals in the time-frequency domain were analyzed by ELM to estimate each of the systolic BP (SBP), mean BP (MBP), and diastolic BP (DBP). The rest of the paper is organized as follows. Section 2 presents the utilized dataset and the employed methodology is given in Section 3. Results and discussion are presented in Section 4 and Section 5 concludes the outcomes of this study.

2. Cuffless Blood Pressure Estimation Dataset

In this study the utilized Cuffless Blood Pressure Estimation Dataset was created in [15] from the Multiparameter Intelligent Monitoring in Intensive Care (MIMIC) waveform database of physionet.org and published by UCI [25]. This dataset consists of clean and validated ECG, PPG, and arterial BP (ABP) signals for 4254 different records, and a part from a signal with a length of 10 s is illustrated in Figure 1.

As seen in Figure 1, ABP is a dynamic parameter that is changing with each heartbeat [13]. Additionally, PPG and ECG signals in this dataset are from the fingertip and channel II, respectively. The sampling frequency of all signals is 125 Hz. An ABP sample is given in Figure 2. As seen in this figure, the ABP varies between the SBP and DBP [15].

3. Applied methodology

The employed methodology is summarized in Figure 3. The proposed methods in estimation of BP (SBP, MBP, and DBP) in the literature focused on feature extraction methods in PPG and/or ECG signals. While the proposed methods in the literature were generally utilized for both PPG and ECG signals together, in this study, ECG and PPG signals were employed separately and/or together.

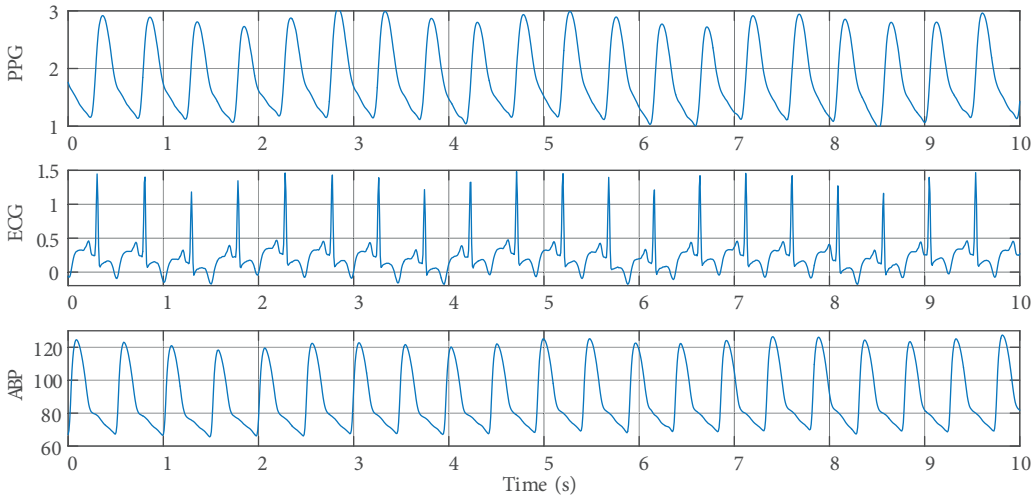

Figure 1. A sample from the employed dataset.

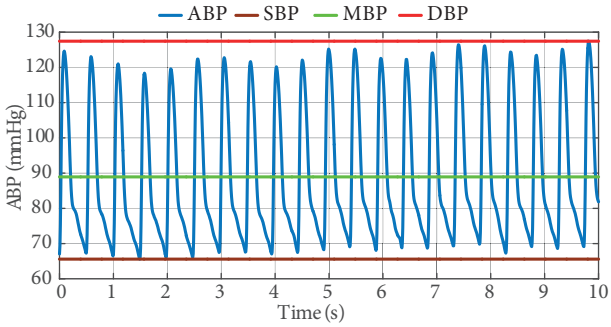

Figure 2. A sample from the employed ABP signal.

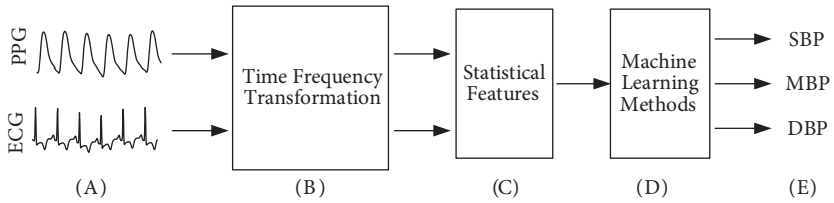

Figure 3. Employed methodology.

3.1. Feature extraction

The frequency content of many biological signals can change with time swiftly. The traditional Fourier transform techniques are not sufficient to analyze the spectral content of these signals that vary with time. By mapping a single direction time or frequency function, the time-frequency representation of a signal can localize the energy of the signal both in the frequency and time directions [26,27]. Many biomedical signals are nonstationary, so the time-frequency analysis of them has been more advantageous than using only time or frequency analysis [28]. The time-frequency energy distribution of biomedical signals exhibits some distinct patterns during abnormality phases, which may be used for event characterization.

Since PPG, ABP, and ECG signals are nonstationary signals, time-frequency analysis was performed to

extract the features in them. To process the data, the spectrogram, which is the magnitude squared of the short time Fourier transform (STFT) of a signal, was employed [29]. In the continuous case, the STFT of a signal, such as x(t), can be defined as:

$$STFT\left\{x\left(t\right)\right\}\left(\tau,\omega\right)=X\left(\tau,\omega\right)=\int_{-\infty}^{+\infty}x\left(t\right)w(t-\tau)e^{-j\omega t}dt \tag{1}$$

where w(t) is the window function that slides along the time axis, resulting in the two-dimensional representation of a signal so that one dimension is time (τ) and the other is frequency (ω). In this paper, the Blackman window with different width sizes was used. The following equation defines the Blackman window of length N [30]:

$$w\left(n\right)=0.42-0.5\cos\left(\frac{2\pi n}{N-1}\right)+0.08\cos\left(\frac{4\pi n}{N-1}\right),\ \ 0\leq n\leq M-1, \tag{2}$$

where N shows the length of the Blackman window and $M = N/2$ if N is even and $M = (N+1)/2$ if N is odd. The employed Blackman window and two of the other popular windows (the Hamming and Hanning windows) in both time and frequency domains (window sizes: N = 64) are given in Figure 4.

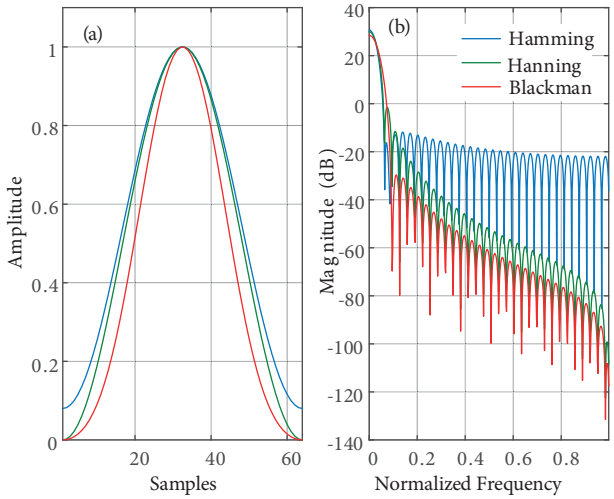

Figure 4. Some popular window types in (a) time and (b) frequency domains.

As seen in Figure 4, the Blackman window provides a narrower window in the time domain and a wider window in the frequency domain compared with the Hamming and Hanning windows [30]. The chosen window widths are 0.25 s, 0.50 s, 0.75 s, 1.00 s, 1.50 s, 2 s, 2.50 s, and 5 s. The number of overlapped points was chosen as 20% of the window width. As expressed in Section 2, the lengths of the employed signals in the dataset are 10 s. Therefore, the window lengths are chosen accordingly to have 1/40 (0.25 s) to 1/2 (5 s) of the lengths of the signals. In this way, the acceptable window length of the signals was assessed. The ECG signal was also expanded by zero padding to have 1000 points per second in order to extract features for narrow frequency bands of the ECG signal. The magnitude squared of the STFT gives the spectrogram of the signal x(t), defined as [31]:

$$\text{spectrogram}\left\{x\left(t\right)\right\}\left(\tau,\omega\right)=\left|X\left(\tau,\omega\right)\right|^{2} \tag{3}$$

After signal processing, some features, which are the minimum, maximum, mean, and standard deviation for each windowed signal, were extracted and used as input for the ELM. These extracted features were employed to estimate SBP, MBP, and DBP by ELM.

3.2. Extreme learning machines (ELMs)

Th ELM is a training method for a single hidden layer feedforward neural network (SLFN) and the output of an SLFN can be calculated as follows [32]:

$$y = \sum_{j=1}^{m} \beta_j g\left(\sum_{i=1}^{n} w_{i,j} x_i + b_j\right) \tag{4}$$

where y, x_i, and n stand for the output and inputs of the network and the number of features in the input, respectively. In an ELM, the weights in the input layer ($w_{i,j}$) and biases of the neurons in the hidden layer (b_j) are assigned arbitrarily and the activation function ($g(.)$) and the number of neurons in the hidden layer (m) are user-defined parameters. By using inputs and outputs in the training dataset, each $g(\sum_{i=1}^{n} w_{i,j} x_i + b_j)$ value is known since some of them are arbitrarily assigned and the others are user-defined parameters. Then the only unknown weights in the output layer (β_j) are calculated analytically in the training stage based on achieving the minimum approximation error by linear algebra:

$$H\beta = y \tag{5}$$

where H, which is also called the hidden matrix, is calculated by

$$H\left(w_{i,j},\, b_j,\, x_i\right) = \begin{bmatrix} g(w_{1,1}x_1 + b_1) & \cdots & g(w_{1,m}x_m + b_m) \\ \vdots & \ddots & \vdots \\ g(w_{n,1}x_n + b_1) & \cdots & g(w_{n,m}x_m + b_m) \end{bmatrix} \tag{6}$$

The weights in the output layer can be calculated by using the inverse of the H matrix by the Moore–Penrose generalized inverse method (H^+) as follows [33]:

$$\hat{\beta} = H^+ y \tag{7}$$

As can be seen from Eq. (7), the optimal weights in the hidden layer can be calculated analytically with an extremely high speed. Additionally, presented papers showed that the ELM also has high generalization capacity [32,34–36].

3.3. Validation metrics

Obtained results by ELM were compared with some popular machine learning methods such as the linear regression (LR), generalized regression neural network (GRNN), k nearest neighbor regression (kNNR), ridge regression (Ridger), least absolute shrinkage and selection operator regression (LASSOR), partial least squares regression (PLSR), and Gaussian process regression (GPR) methods in terms of both accuracy and process time (training and testing time) [37]. The mean absolute relative error (MARE), mean absolute error (MAE), root

mean square error (RMSE), and mean absolute percentage error (MAPE) can be calculated as follows:

$$MARE = \frac{1}{n}\sum_{i=1}^{n}\left|\frac{f_i - y_i}{y_i}\right| \tag{8}$$

$$MAE = \frac{1}{n}\sum_{i=1}^{n}|f_i - y_i| \tag{9}$$

$$RMSE = \sqrt{\frac{1}{n}\sum_{i=1}^{n}(f_i - y_i)^2} \tag{10}$$

$$MAPE = \frac{100}{n}\sum_{i=1}^{n}\left|\frac{f_i - y_i}{y_i}\right| \tag{11}$$

where f, y, n, and E are forecasted (estimated) value, true (observed) value, number of samples, and expected value, respectively. Furthermore, each test was performed by MATLAB according to 12-fold cross-validation in order to achieve fairer results, which are less dependent on the order of the samples.

4. Results and discussion

In the validation stage, first the structure of the single hidden neural network was optimized. Later, the proposed approach was assessed from many perspectives and finally results achieved by the proposed approach were compared with the results of some other machine learning methods and results reported in the literature.

4.1. Optimization stage

In a single hidden layer neural network, both the activation function and number of neurons in the hidden layer must be optimized in order to achieve higher accuracies. Generally, optimization is done by trials. In this study the optimal number of neurons in the hidden layer was chosen as 5, 10, 15, 20, 25, and 30, while the optimal activation function was tested for the sigmoid, sine, radial basis, hard limit, symmetric hard limit, symmetric saturating linear, hyperbolic tangent sigmoid, triangular basis, positive linear, and pure linear activation functions. This optimization was done for determining the optimal network structure for estimating SBP, MBP, and DBP in each dataset (PPG, ECG, and PPG + ECG). For instance, the optimization of network parameters in the PPG dataset for estimating SBP is illustrated in Figure 5. The number of neurons in the hidden layer and the activation function were determined according to the obtained accuracies. As seen in Figure 5, the optimum activation function and the number of neurons are the radial basis function and 10, respectively.

4.2. Subject-free results

In this stage, each sample that belonged to a subject was combined and reordered arbitrarily. Then the ELM was employed in order to estimate SBP, MBP, and DBP. Obtained error rates based on 12-fold cross-validation are summarized in Table 1. As seen for subject-free results in Table 1, the SBP, MBP, and DBP can be estimated more accurately by using PPG signals. Additionally, in order to assess the performance of the ELM, some other machine learning methods, which are GRNN, LR, kNN, RIDGER, LASSOR, kSmooth, PLSR, and GPR, were

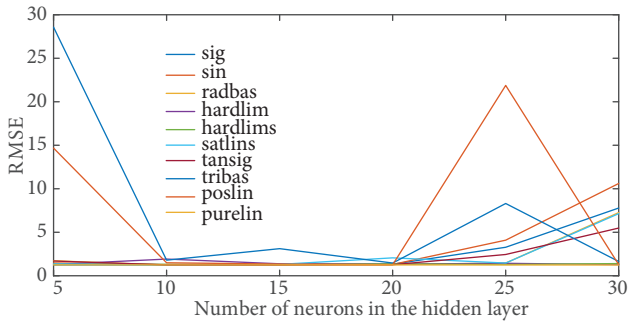

Figure 5. Optimizing the structure of the single hidden layer artificial neural network.

employed in estimating SBP, MBP, and DBP by the PPG + ECG dataset and obtained RMSEs based on 12-fold cross-validation are given in Table 2.

Table 1. Obtained subject-free error rates by ELM.

Dataset	Parameter	MAE	RMSE	MAPE	MARE
PPG	SBP	4.253	5.234	6.682	0.067
	MBP	3.579	4.457	4.382	0.044
	DBP	3.946	4.933	3.997	0.040
ECG	SBP	4.364	5.477	6.803	0.068
	MBP	4.038	5.066	4.905	0.049
	DBP	4.570	5.728	4.570	0.046
PPG + ECG	SBP	4.371	5.478	6.825	0.068
	MBP	3.639	4.562	4.405	0.044
	DBP	3.953	4.935	4.000	0.040

Table 2. Obtained RMSE by some popular machine learning methods for PPG + ECG dataset.

Employed machine learning method	Obtained RMSE in estimating parameter		
	SBP	MBP	DBP
GRNN	5.819	5.015	5.348
LR	5.825	5.165	5.427
kNN	7.234	6.275	6.545
RIDGER	5.848	5.239	5.541
LASSOR	5.848	5.239	5.541
kSmooth	5.886	5.027	5.35
PLSR	6.62	6.44	7.169
GPR	16.407	20.654	27.731

As seen in Table 2, the minimum RMSEs were achieved by GRNN in estimating each of the parameters. Achieved RMSEs are 5.819, 5.015, and 5.348 in estimating the SBP, MBP, and DBP, respectively. Since obtained RMSEs by the ELM in PPG + ECG in estimating SBP, MBP, and DBP are 5.478, 4.562, and 4.935, respectively (see Table 1), it can be said that the ELM showed higher success in estimating ABP.

In order to assess the effectivity of using exacting features from the signals in the time-frequency domain, some statistical features, which are given in Table 3, were extracted in the time and frequency domains of the signals. Obtained error rates by the ELM and other employed machine learning methods are given in Table 4. As seen Tables 1, 2, and 4, the best results were obtained by the features that were extracted from the signals in the time-frequency domain.

Table 3. Extracted statistical features.

Domain	Statistical features
Time domain	Energy, mean, standard deviation, maximum, minimum, kurtosis, skewness
Frequency domain	Mean, standard deviation, kurtosis, skewness

Table 4. Achieved error rates with PPG and/or ECG datasets.

	ML Methods	SBP			MBP			DBP		
		MARE	MAE	RMSE	MARE	MAE	RMSE	MARE	MAE	RMSE
PPG	ELM	0.11	6.84	9.05	0.12	9.37	11.27	0.14	19.26	23.77
	GRNN	0.15	8.76	12.57	0.16	14.23	18.44	0.19	26.35	33.02
	LR	0.11	6.86	9.27	0.12	10.55	13.45	0.14	19.60	24.17
	kNNR	0.15	8.96	12.94	0.17	14.53	18.87	0.20	26.88	33.71
	RIDGER	0.11	6.85	9.26	0.12	10.56	13.48	0.14	19.60	24.17
	LASSOR	0.11	6.89	9.28	0.12	10.55	13.47	0.14	19.59	24.15
	PLSR	0.13	7.70	10.43	0.14	12.17	15.64	0.16	21.63	26.84
	GPR	0.96	55.53	56.81	0.96	84.26	86.28	0.96	136.07	139.97
ECG	ELM	0.11	6.99	9.37	0.12	9.90	11.81	0.14	19.48	24.18
	GRNN	0.15	9.14	13.13	0.17	15.14	19.55	0.21	28.04	34.77
	LR	0.12	7.10	9.47	0.12	10.90	13.81	0.14	19.58	24.19
	kNNR	0.15	9.23	13.30	0.17	15.29	19.77	0.21	28.30	35.10
	RIDGER	0.12	7.06	9.42	0.12	10.86	13.74	0.14	19.53	24.11
	LASSOR	0.12	7.08	9.44	0.12	10.86	13.73	0.14	19.51	24.09
	PLSR	0.20	11.94	16.17	0.20	17.96	23.65	0.22	30.84	39.83
	GPR	0.99	57.40	58.28	0.99	86.92	88.23	0.99	140.13	142.80
PPG & ECG	ELM	0.11	6.93	9.30	0.12	8.86	11.92	0.14	19.43	24.05
	GRNN	0.17	15.14	19.58	0.15	9.03	13.05	0.21	28.04	34.92
	LR	0.12	10.56	13.47	0.11	6.97	9.39	0.14	19.21	23.86
	kNNR	0.17	15.15	19.58	0.15	9.03	13.05	0.21	28.05	34.93
	RIDGER	0.12	10.58	13.52	0.11	6.96	9.39	0.14	19.22	23.88
	LASSOR	0.12	10.55	13.47	0.12	7.00	9.42	0.14	19.15	23.78
	PLSR	0.14	12.50	16.27	0.13	7.87	10.58	0.16	22.10	28.18
	GPR	1.00	87.31	88.49	1.00	57.66	58.47	1.00	140.72	143.18

4.3. Subject-based results

In order to investigate the subject-based accuracy, datasets that belonged to five subjects were randomly selected from the Cuff-Less Blood Pressure Estimation Dataset [15]. Obtained accuracies based on 12-fold cross-validation are summarized in Table 5.

Table 5. Obtained error rates for subject-based signals.

Dataset	Parameter	MAE	RMSE	MAPE	MARE
PPG	SBP	1.039	1.345	1.630	0.016
	MBP	1.012	1.387	1.222	0.012
	DBP	1.384	1.806	1.378	0.014
ECG	SBP	1.065	1.388	1.670	0.017
	MBP	1.032	1.419	1.246	0.012
	DBP	1.390	1.821	1.388	0.014
PPG + ECG	SBP	1.054	1.374	1.649	0.016
	MBP	1.008	1.368	1.218	0.012
	DBP	1.383	1.818	1.378	0.014

As seen in Table 5, obtained error rates are close to each other. The results in this table belonging to the windows that are 1 s long (125 samples per a window). Therefore, in order to investigate the relationship between window length and obtained accuracy, various windows with different window lengths were employed and obtained accuracies in each case are summarized in Table 6 based on 12-fold cross-validation. Note that there are 125 samples in 1 s.

As seen in Table 6, the lowest RMSEs were achieved in estimating SBP, MBP, and DBP when the lengths of windows were 2.5, 5, and 5 s, respectively. Another interesting obtained result is that the RMSEs obtained with the PPG dataset were the lowest in comparison to RMSEs obtained with the ECG and PPG + ECG datasets. In order to visualize these results, the DBP of an arbitrarily selected subject (5th subject in part 2) was estimated for various cases that used different windows lengths, and obtained RMSEs based on 12-fold cross-validation are given in Figure 6.

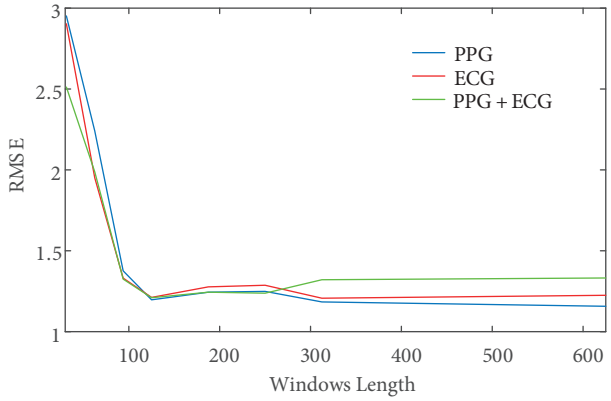

Figure 6. Obtained RMSEs according to window lengths.

The results in Figure 6 well suit the results in Table 6. Furthermore, Bracic and Stefanovska reported that some subfrequencies in a blood flow signal, which are given in Table 7, are associated with different

physiological activities [38]. In order to assess the relationship between these reported subbands, the ECG signal time-frequency domain was filtered and the statistical features were extracted from these filtered signals. Obtained RMSEs are given in Table 8 based on 12-fold cross-validation. The results in Tables 7 and 8 show that the most effective subband in estimating SBP, MBP, and DBP is the heart activity, as expected.

Table 6. Obtained RMSEs based on employed window length.

Window length (s)	Parameter	PPG	ECG	PPG + ECG
0.25	SBP	3.767	3.064	2.402
	MBP	3.502	2.803	2.357
	DBP	2.952	2.903	2.512
0.5	SBP	2.101	2.236	2.057
	MBP	1.933	1.681	1.610
	DBP	2.241	1.951	1.988
0.75	SBP	1.254	1.240	1.222
	MBP	1.200	1.279	1.248
	DBP	1.376	1.331	1.325
1	SBP	1.171	1.246	1.246
	MBP	1.046	1.134	1.171
	DBP	1.197	1.212	1.210
1.5	SBP	1.113	1.139	1.100
	MBP	1.026	1.018	1.081
	DBP	1.244	1.277	1.244
2	SBP	1.113	1.145	1.139
	MBP	0.952	0.969	0.959
	DBP	1.249	1.287	1.238
2.5	SBP	1.081	1.074	1.162
	MBP	0.964	0.950	0.977
	DBP	1.184	1.207	1.321
5	SBP	1.135	1.030	1.158
	MBP	0.631	0.637	0.635
	DBP	1.157	1.225	1.332

4.4. Subject-based time-ordered results

Since the motivation of writing this paper is to propose an approach that can be employed in order to estimate SBP, MBP, and DBP simultaneously, each sample that was extracted from the PPG, ECG and PPG + ECG in the time-frequency domain was estimated based on its previous samples for each particular subject and obtained mean accuracies are listed in Table 9.

As seen in Table 9, lower error rates were achieved while using each subject-based dataset in a time-ordered way instead of employing a batch approach. Obtained RMSEs in estimating DBP from PPG are given in Figure 7.

Table 7. Frequency subbands [38].

Frequency band (Hz)	Physiological activity
0.6–1.6	Heart activity
0.16–0.4	Respiratory activity
0.06–0.16	Myogenic activity
0.02–0.06	Neurogenic activity
0.0095–0.02	Metabolic activity

Table 8. Obtained RMSEs based on frequency subbands and window lengths.

Window length (s)	Parameter	Frequency bands (Hz)				
		0.6–1.6	0.16–0.4	0.06–0.16	0.02–0.06	0.0095–0.02
0.25	SBP	2.884	2.827	2.737	2.731	2.628
	MBP	2.675	2.695	2.595	2.450	2.381
	DBP	2.724	2.742	2.732	2.701	2.627
0.5	SBP	2.265	2.127	2.090	1.883	1.795
	MBP	1.807	1.755	1.667	1.666	1.587
	DBP	1.870	1.878	1.871	1.868	1.868
0.75	SBP	1.238	1.233	1.228	1.345	1.242
	MBP	1.357	1.347	1.349	1.339	1.325
	DBP	1.328	1.326	1.327	1.323	1.328
1	SBP	1.205	1.207	1.240	1.207	1.236
	MBP	1.431	1.346	1.377	1.299	1.120
	DBP	1.204	1.217	1.205	1.212	1.210
1.5	SBP	1.096	1.098	1.100	1.095	1.118
	MBP	0.990	0.991	0.992	0.988	0.993
	DBP	1.234	1.229	1.236	1.236	1.268
2	SBP	1.132	1.127	1.136	1.129	1.137
	MBP	0.918	0.949	0.929	0.893	0.960
	DBP	1.240	1.201	1.208	1.204	1.284
2.5	SBP	1.075	1.081	1.081	1.081	1.077
	MBP	0.936	0.935	0.935	0.935	0.917
	DBP	1.196	1.199	1.287	1.201	1.299
5	SBP	1.165	1.167	1.166	1.163	1.151
	MBP	0.648	0.649	0.649	0.661	0.653
	DBP	1.166	1.172	1.175	1.183	1.167

4.5. Comparison with the literature

In order to validate the feasibility of the proposed approach, obtained results must also be confirmed with reported results in the literature. Some reported errors in estimating SBP, MBP, and DBP are given in Table 10.

Table 9. Obtained subject-based error rates in employing datasets according to time order.

Dataset	Parameter	MAE	RMSE	MAPE	MARE
PPG	SBP	1.050	1.574	1.617	0.016
	MBP	0.798	1.021	0.991	0.010
	DBP	1.019	1.398	1.088	0.011
ECG	SBP	0.915	1.212	1.410	0.014
	MBP	1.241	2.346	1.553	0.016
	DBP	0.942	1.269	1.005	0.010
PPG + ECG	SBP	0.827	1.033	1.277	0.013
	MBP	0.867	1.191	1.080	0.011
	DBP	1.092	1.565	1.163	0.012

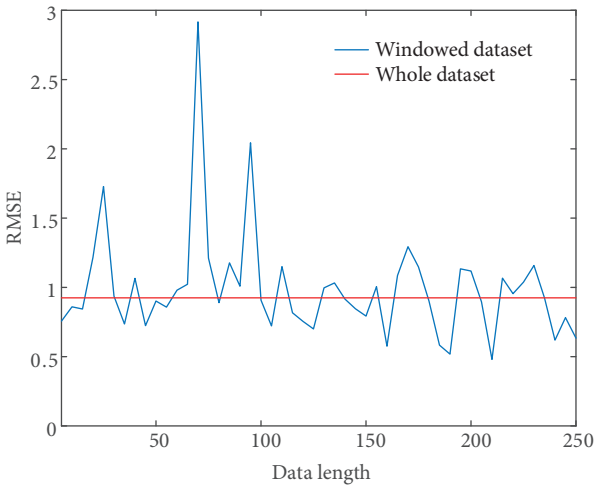

Figure 7. Obtained RMSEs according to data lengths.

In Table 10, AE is the absolute error (mmHg), μ shows MBP error (mmHg), r is correlation coefficient, MSE MBP is the MBP squared error (mmHg), and MAD is MBP absolute difference (mmHg). It is obvious from Table 10 that RMSEs obtained by the proposed approach are lower than the achieved ones (see Table 9). The proposed approach can be acceptable based on the comparison between achieved results in this study (see Tables 1, 5, 6, and 9) and reported results in the literature.

The proposed approach has some major improvements over the presented approaches in the literature. Just measuring ECG or PPG is enough to estimate SBP, MBP, and DBP. Moreover, it was reported by Ding and Zhang that some presented estimation methods can only provide SBP, MBP, or DBP, but in the proposed method the three of them can be provided simultaneously [13]. Furthermore, achieved accuracies in the estimation of SBP, MBP, and DBP in the present paper are Grade A based on the British Hypertension Society standards [15]. Additionally, obtained errors in this study are also lower than the standards of the Association for the Advancement of Medical Instrumentation, in which MAE and STD must be lower than 5 mmHg and 8 mmHg for both SBP and DBP [5,16]. Further investigations should be carried out to determine more relevant statistical properties for achieving lower error rates. On the other hand, extracting features from the signals in the time-

Table 10. Reported error rates in estimating SBP, MBP, and DBP in the literature.

Ref.	#Subjects	Signal	Method	Accuracy		
				SBP	MBP	DBP
[1]	11	ECG & PPG	PTT + ECG R-peak Detection + PPG peak detection	AE = 14.83–18.29		AE = 8.22–12.09
[4]	55	PPG & ECG	Delta PAT and delta HR	RMSE = 5.21 r = 0.691		RMSE = 4.32 r = 0.578
[5]	25	PPG & ECG	PTT and Hilbert–Huang transform	μ = 0.44 STD = 3.85 r = 0.71		μ = 0.93 STD = 1.84 r = 0.69
[6]	5	PPG	Cardiovascular parameters + multiple regression		r = 0.71	
[7]	96	PPG	Acceleration pulse wave	r = 0.89 STD = 8.2		
[8]	4	ECG & PPG	PAT + LR PTT + LR	E = 2.7–16 E = 12–25		
[13]	27	ECG & PPG	PPG intensity ratio + PTT	μ = −0.37 STD = 5.21 MAD = 4.09	μ = −0.08 STD = 4.06 MAD = 3.18	μ = −0.18 STD = 4.13 MAD = 3.18
[15]	-	ECG & PPG	Physiological parameters + SVM	MAE = 6.34 STD = 8.45	MAE = 7.52 STD = 9.54	MAE = 12.38 STD = 16.17
[16]	25	ECG & PPG	PAT and HR	μ = 0.41 MSE = 70.05		μ = 0.07 MSE = 35.08
[39]	41	ECG & PPG	PTT	μ = 1.4 STD = 10.2		μ = 2.1 STD = 7.3
[40]	23	ECG & PPG	PTT	μ = 0.52 STD = 3.3 r = 0.983		

frequency domain is a more time-consuming process than extracting the features in any of the time or frequency domains of the signals.

5. Conclusion

BP is one of the most important health parameters and unfortunately, for more than a century, it has generally been measured by mercury sphygmomanometer. Since the measurement procedure by mercury sphygmomanometer is a hard and time-consuming process, alternative methods have been presented in the literature, which are generally based on measuring both PPG and ECG and estimating BP based on these records. In this study, a simple, effective, and subject-free methodology that shows high accuracy (low error) by using PPG and ECG separately or both ECG and PPG signals together was presented. In the proposed method, statistical features were extracted from the signals in the time-frequency domain. Later, extracted features were employed to estimate SBP, MBP, and DBP by ELM. Achieved results showed that by the proposed approach only a PPG or an ECG signal is enough to estimate SBP, MBP, and DBP. Moreover, each of these BP types can be provided simultaneously.

References

[1] Goli S, Jayanthi T. Cuff less continuous non-invasive blood pressure measurement using pulse transit time measurement. International Journal of Recent Development in Engineering and Technology 2014; 2: 86-91.

[2] He FJ, MacGregor GA. Blood pressure is the most important cause of death and disability in the world. Eur Heart J 2007; 9 (Suppl.): 23-28.

[3] European Community. Sphygmomanometers. Brussels, Belgium: EC, 2009. Available online at https://ec.europa.eu/health/scientific_committees/opinions_layman/sphygmomanometers/en/index.htm.

[4] Mottaghi S, Moradi MH, Roohisefat L. Cuffless blood pressure estimation during exercise stress test. International Journal of Bioscience, Biochemistry and Bioinformatics 2012; 2: 394-397.

[5] Choi Y, Zhang O, Ko S. Noninvasive cuffless blood pressure estimation using pulse transit time and Hilbert-Huang transform. Comput Electr Eng 2013; 39: 103-111.

[6] Fukushima H, Kawanaka H, Bhuiyan MS, Oguri K. Cuffless blood pressure estimation using only photoplethysmography based on cardiovascular parameters. In: 35th Annual International Conference of the IEEE in Engineering in Medicine and Biology Society; 3–7 July 2013; Osaka, Japan. New York, NY, USA: IEEE. pp. 2132-2135.

[7] Suzuki S, Oguri K. Cuffless and non-invasive systolic blood pressure estimation for aged class by using a photoplethysmograph. In: 30th Annual International Conference of the IEEE in Engineering in Medicine and Biology Society; 20–25 August 2008; Vancouver, BC, Canada. New York, NY, USA: IEEE. pp. 1327-1330.

[8] Deb S, Nanda C, Goswami D, Mukhopadhyay J, Chakrabarti S. Cuff-less estimation of blood pressure using pulse transit time and pre-ejection period. In: International Conference on Convergence Information Technology; 21–23 November 2007; Gyongju, South Korea. New York, NY, USA: IEEE. pp. 941-944.

[9] Payne RA, Symeonides CN, Webb DJ, Maxwell SRJ. Pulse transit time measured from the ECG: an unreliable marker of beat-to-beat blood pressure. J Appl Physiol 2006; 100: 136-141.

[10] Poon CCY, Zhang YT. Cuff-less and noninvasive measurements of arterial blood pressure by pulse transit time. In: 27th Annual International Conference of the Engineering in Medicine and Biology Society; 17–18 January 2006; Shanghai, China. New York, NY, USA: IEEE. pp. 5877-5880.

[11] Geddes LA, Voelz MH, Babbs CF, Bourland JD, Tacker WA. Pulse transit time as an indicator of arterial blood pressure. Psychophysiology 1981; 18: 71-74.

[12] Gesche H, Grosskurth D, Küchler G, Patzak A. Continuous blood pressure measurement by using the pulse transit time: comparison to a cuff-based method. Eur J Appl Physiol 2012; 112: 309-315.

[13] Ding XR, Zhang YT. Cuff-less continuous blood pressure estimation with pulse transit time and photoplethysmogram intensity ratio. In: International Biomedical Engineering Conference 2014 Jointly with uHealthcare; 20–22 November 2014; Gwangju, Korea. p. 351

[14] Fung P, Dumont G, Ries C, Mott C, Ansermino M. Continuous noninvasive blood pressure measurement by pulse transit time. In: 26th Annual International Conference of the IEEE in Engineering in Medicine and Biology Society; 1–5 September 2004; San Francisco, CA, USA. New York, NY, USA: IEEE. pp. 738-741.

[15] Kachuee M, Kiani MM, Mohammadzade H, Shabany M. Cuff-less high-accuracy calibration-free blood pressure estimation using pulse transit time. In: IEEE International Symposium on Circuits and Systems; 24–27 May 2015; Lisbon, Portugal. New York, NY, USA: IEEE. pp. 1006-1009.

[16] Cattivelli FS, Garudadri H. Noninvasive cuffless estimation of blood pressure from pulse arrival time and heart rate with adaptive calibration. In: Sixth International Workshop on Wearable and Implantable Body Sensor Networks; 3–5 June 2009; Berkeley, CA, USA: IEEE. pp. 114-119.

[17] Liu Q, Poon CCY, Zhang YT. Time–frequency analysis of variabilities of heart rate, systolic blood pressure and pulse transit time before and after exercise using the recursive autoregressive model. Biomed Signal Process Control 2011; 6: 364-369.

[18] Ahlstrom C, Johansson A, Uhlin F, Länne T, Ask P. Noninvasive investigation of blood pressure changes using the pulse wave transit time: a novel approach in the monitoring of hemodialysis patients. J Artif Organs 2005; 8: 192-197.

[19] Johansson A, Ahlstrom C, Lanne T, Ask P. Pulse wave transit time for monitoring respiration rate. Med Biol Eng Comput 2006; 44: 471-478.

[20] Sezgin N. A new hand finger movements' classification system based on bicoherence analysis of two-channel surface EMG signals. Neural Comput Appl (in press).

[21] Wang Y, Cao F, Yuan Y. A study on effectiveness of extreme learning machine. Neurocomputing 2011; 74: 2483-2490.

[22] Sattar AMA, Ertuğrul ÖF, Gharabaghi B, McBean EA, Cao J. Extreme learning machine model for water network management. Neural Comput Appl (in press).

[23] Bin Huang G, Wang DH, Lan Y. Extreme learning machines: a survey. Int J Mach Learn Cyb 2011; 2: 107-122.

[24] Ertuğrul ÖF, Altun Ş. Developing correlations by extreme learning machine for calculating higher heating values of waste frying oils from their physical properties. Neural Comput Appl 2017; 28: 3145-3152.

[25] Bache K, Lichman M. UCI Machine Learning Repository. Irvine, CA, USA: University of California, 2013.

[26] Cohen L. Time-frequency distributions-a review. P IEEE 1989; 77: 941-981.

[27] Sejdić E, Djurović I, Jiang J. Time–frequency feature representation using energy concentration: an overview of recent advances. Digit Signal Process 2009; 19: 153-183.

[28] Wacker H, Witte M. Time-frequency techniques in biomedical signal analysis. Methods Inf Med 2013; 52: 279-296.

[29] Portnoff M. Time-frequency representation of digital signals and systems based on short-time Fourier analysis. IEEE T Acoust 1980; 28: 55-69.

[30] Podder P, Khan TZ, Khan MH, Rahman MM. Comparative performance analysis of Hamming, Hanning and Blackman window. International Journal of Computer Applications 2014; 96: 975-8887.

[31] Yuan Y, Xun G, Jia K, Zhang A. A multi-view deep learning method for epileptic seizure detection using short-time Fourier transform. In: 8th ACM International Conference on Bioinformatics, Computational Biology, and Health Informatics; 20–23 August 2017; Boston, MA, USA. New York, NY, USA: ACM. pp. 213-222.

[32] Huang GB, Zhu Q, Siew CK. Extreme learning machine: theory and applications. Neurocomputing 2006; 70: 489-501.

[33] Huang GB. An insight into extreme learning machines: random neurons, random features and kernels. Cognit Comput 2014; 6: 376-390.

[34] Ertuğrul ÖF, Kaya Y. A detailed analysis on extreme learning machine and novel approaches based on ELM. Am J Comput Sci. Eng 2014; 1: 43-50.

[35] Ertuğrul ÖF. Forecasting electricity load by a novel recurrent extreme learning machines approach. Int J Elec Power 2016; 78: 429-435.

[36] Sezgin N. EMG classification in obstructive sleep apnea syndrome and periodic limb movement syndrome patients by using wavelet packet transform and extreme learning machine. Turk J Elec Eng & Comp Sci 2015; 23: 873-884.

[37] Monte-Moreno E. Non-invasive estimate of blood glucose and blood pressure from a photoplethysmograph by means of machine learning techniques. Artif Intell Med 2011; 53: 127-138.

[38] Bracic M, Stefanovska A. Wavelet-based analysis of human blood-flow dynamics. Bull Math Biol 1998; 60: 919-935.

[39] Wong MYM, Poon CCY, Zhang YT. An evaluation of the cuffless blood pressure estimation based on pulse transit time technique: a half year study on normotensive subjects. Cardiovasc Eng 2009; 9: 32-38.

[40] Shriram R, Wakankar A, Daimiwal N, Ramdasi D. Continuous cuffless blood pressure monitoring based on PTT. In: International Conference on Bioinformatics and Biomedical Technology; 16–18 April 2010; Chengdu, China. New York, NY, USA: IEEE. pp. 51-55.